Flange-to-flange double-tee connections subjected to vehicular loading, part 2: Fatigue life assessment

Clay Naito, Robin Hendricks, and Andrew Osborn

Review policy

This paper summarizes the fatigue test program of a PCI-funded research effort to assess the fatigue resistance of welded flange-to-flange connections used in double-tee precast concrete construction. This paper was reviewed by both PCI's Technical Activities and Research and Development Councils in accordance with their review processes.

Flange-to-flange connections have been used for over 50 years in the construction of prestressed concrete double-tee parking structures. The connection provides integrity for the floor by providing shear and axial force transfer and allows a means of achieving vertical alignment between adjacent tees. Connections along the span of the double tee are often designed primarily for shear, while chord connections are designed for tension, compression, and shear.[1]

When the parking deck is subjected to vehicle loads, the double-tee flange undergoes localized deformations at the joint. These include rotation of the first double-tee flange (flange 1), rotation of adjacent double-tee flange (flange 2), axial deformation between the two double-tee flanges, and vertical deformation between the flanges. The magnitude of these deformations is a function of the weight and geometry of the vehicle, the global flexural stiffness of the double tee, the local flexural stiffness of the double-tee flange, the torsional stiffness of the double tee, the stiffness and spacing of connections between the two flanges, and the boundary conditions of the double tees. **Figure 1** illustrates the deformation states. These deformations are generated at the connections as the vehicle passes along the drive aisle transverse to the double-tee span. As a vehicle moves across the deck of the parking structure, the connection can be subjected to a cycle from each axle load. The deformation is typically largest for a given connection when the wheel nearest the connection passes from the double tee on one side of the joint to the double tee on the other side of the joint.

The focus of this study is to determine the fatigue resistance of conventional flange-to-flange connections used in double-tee parking structures subjected to vertical wheel loads. The common detail used currently in the United States consists of steel connectors embedded in adjacent double-tee flanges and fillet welded together using a steel jumper plate

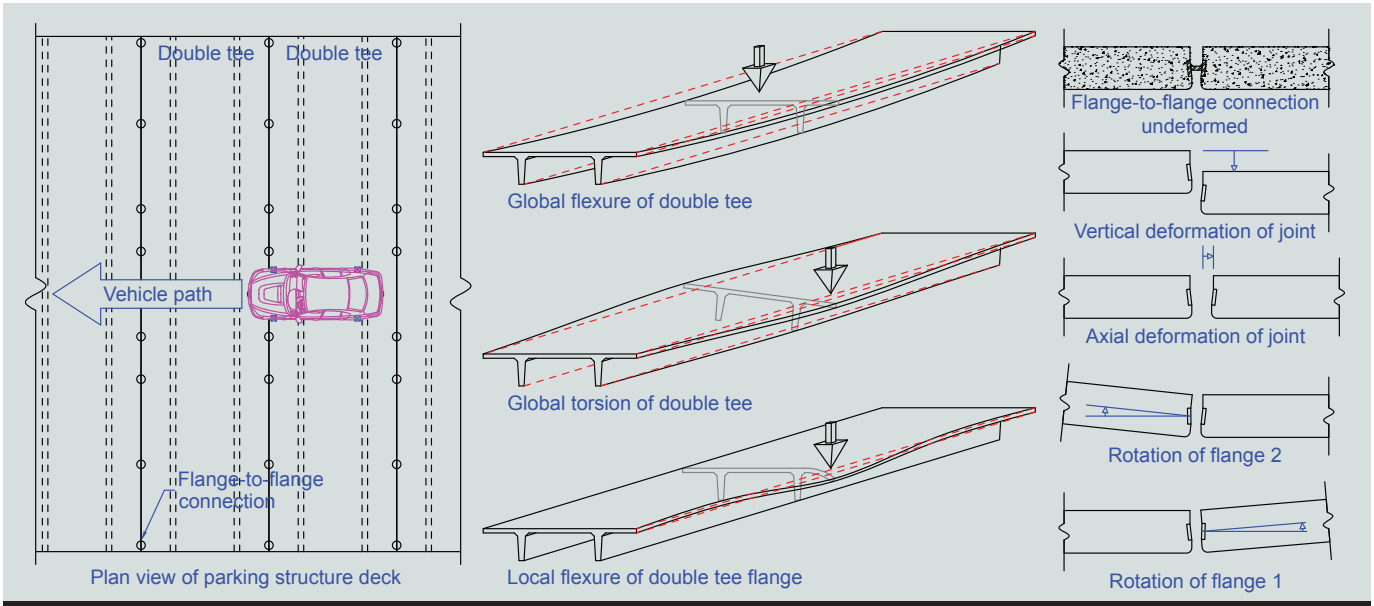

Figure 1. Global and local deformations of double tees and connections.

(**Fig. 2**). These connectors are often fabricated from strap steel plate, stamped and bent to provide in-plane axial, in-plane shear, and out-of-plane shear resistance. As discussed in detail in the companion paper,[2] these deformations can induce high stresses on the root of the fillet weld used in the connection. Due to the relative deformations that occur at the connection and the flexibility of the embedded connector faceplate, this detail is subject to complex stress distribution (Fig. 2).

The fillet-weld detail used in flange-to-flange connections is not classified by the American Institute of Steel Construction (AISC).[3] The closest comparison is the AISC fatigue category F connection (AISC detail 8.2) (**Fig. 3**), because a category F weld is subjected to shear, tension, and bending. As a category F detail, the fatigue life expected by AISC would be negligible. However, the observed longevity of this connection detail in many parking structures indicates that the AISC category S-N curve is not applicable for this connection detail. The flexibility of the faceplate in the flange-to-flange connection results in a more compliant detail and a complex stress field that cannot be analyzed using the nominal stress S-N approach.

A limited amount of applicable fatigue test data is available in the literature.[4,5] Most of the research appears to be related to offshore structures and ship hulls. In offshore structures, tubular braces are welded to tubular support columns via fillet-welded end plates. The fillet welds surrounding these end plates are subjected to combined tension, shear, and bending stresses in a manner not dissimilar to the way flange-to-flange jumper plate welds are stressed. In ship structures, a similar connection is used where the ship stanchions (essentially a type of strut or brace) are attached to the hull. A number of welded conditions have been defined for these structure types.[4] One type of weld is a fillet weld joining two perpendicular plates, with the perpendicular plate subjected to transverse loads. This connection is subject to a number of loading and weld variations where fillet welds can occur on one or both sides. A typical connection is illustrated in Fig. 3.

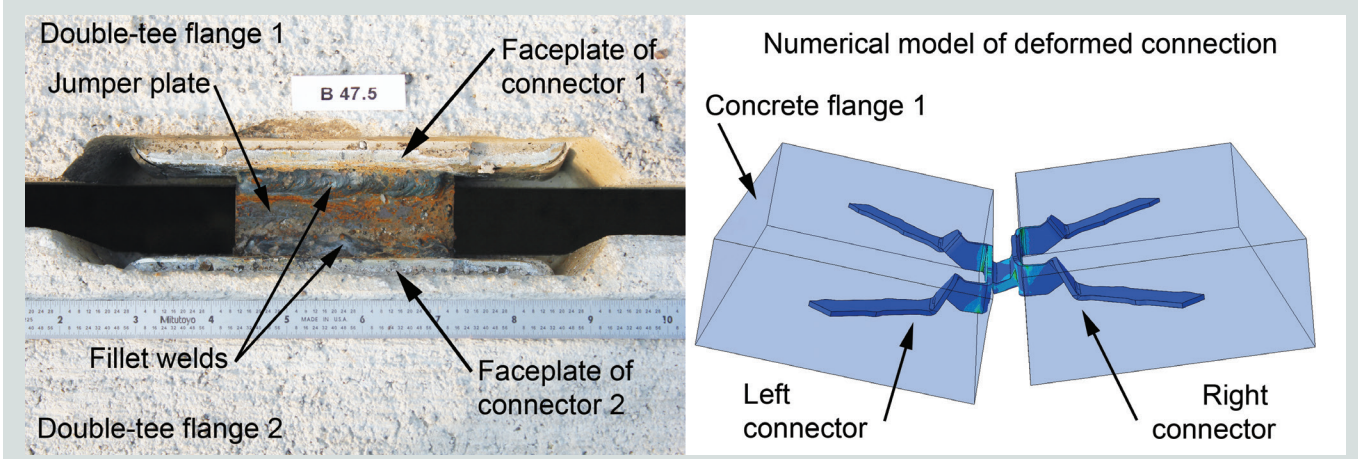

Figure 2. Double-tee flange-to-flange connection detail and stress contours on numerically determined deformed shape.

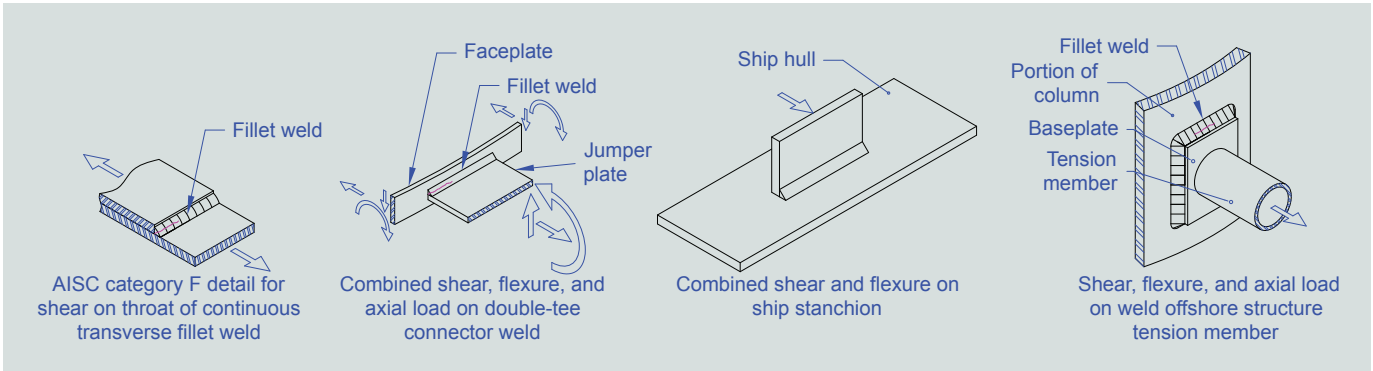

Figure 3. Fillet weld details.

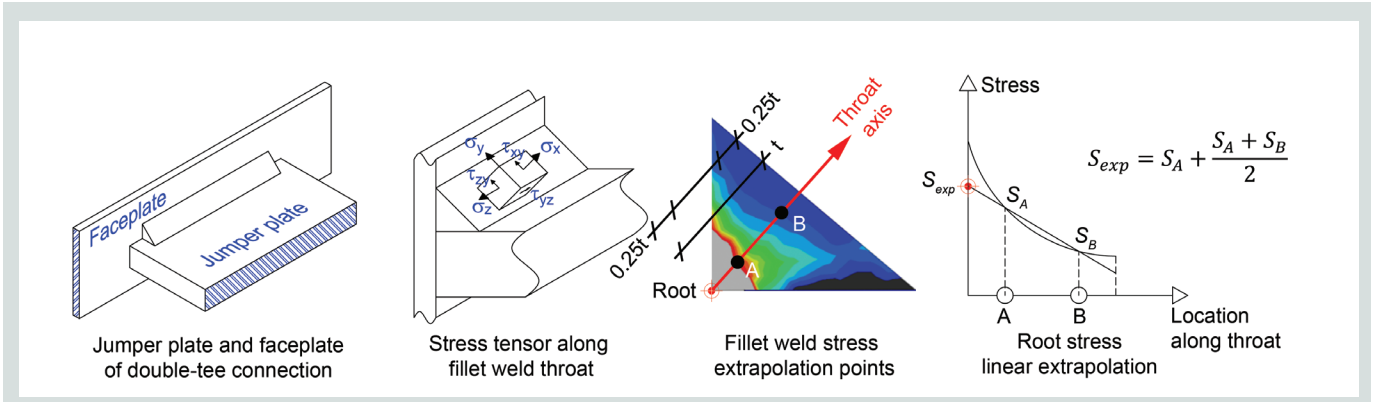

Figure 4. Extrapolation for determination of root stress. Source: adapted from Sorensen et al. (2006). Note: A = quarter point (located closer to the root of the weld) along a line that radiates from the root of the weld to the face of the weld; B = quarter point (located closer to the face of the weld) along a line that radiates from the root of the weld to the face of the weld; S_A = average principal tension stress at the root of the weld at point A; S_B = average principal tension stress at the root of the weld at point B; S_{exp} = extrapolated average principal tension stress at the root of the weld; t = thickness of weld throat; σ_x = normal stress in x-direction; σ_y = normal stress in y-direction; σ_z = normal stress in z-direction; τ_{xy} = shear stress in xy-plane; τ_{xz} = shear stress in xz-plane; τ_{zy} = shear stress in zy-plane.

While the research efforts of both Sorensen et al.[5] and Dimitrakis[4] resulted in S-N fatigue life curves, both details differ from flange-to-flange connections in the supporting component. For the flange connection, the supporting component (the faceplate) is flexible, while the supporting component of the previously evaluated details was large and resulted in a relatively rigid base support. The flange connection weld has a discrete length, while the tension member has a continuous weld. These differences result in a uniform stress distribution along the tension member weld that may be unconservative for double-tee connections.

To assess the fatigue resistance of the double-tee connections, an experimental fatigue test program was conducted. The fatigue life of the weld can be determined by applying cyclic loading to the detail until failure is observed. The literature reports that the ship test series weld failures and the offshore brace weld failures tend to initiate at the root of the fillet weld. This is contrary to fatigue failures in other fillet welds, which tend to initiate at the toe of the weld. The corresponding stress range at the root must be determined for the given applied loading. Due to the complexity of the stress field, the stress at the root is determined using a stress concentration factor (SCF) approach.

Stress concentration factor

To assess the likelihood of fatigue-induced cracking, the level of stress induced at the root of the weld must be determined. Because the stress at the root cannot be physically measured due to its location, the stress must be determined in an alternative manner. Finite element analysis (FEA) of the detail can be used; however, the geometry of the root of the weld creates a singularity in the model. A singularity in a FEA model results in a continual increase in stress at that point as the mesh is refined. This phenomenon is due to the FEA approach and is not a function of what is physically occurring in the weld. To overcome this modeling issue, an SCF approach can be used in place of the point stress range at the root (**Fig. 4**). Sorensen et al.[5] developed two SCF approaches for welds used in offshore structures: a simplified SCF4 approach and a more complex SCF5 approach. The SCF5 approach is adopted for this study due to its improved accuracy over SCF4. SCF5 represents the largest principal stress at the root extrapolated from the six components of stress. The normal stresses (σ_x, σ_y, σ_z) and the shear stresses (τ_{xy}, τ_{xz}, τ_{yz}) are calculated at the quarter points along a line that radiates from the root of the weld to the face of the weld (Fig. 4). These values are then linearly extrapolated (see S_{exp} in Fig. 4) to compute the six

components of stress at the root of the weld ($\sigma_{x,exp}$, $\sigma_{y,exp}$, $\sigma_{z,exp}$, $\tau_{xy,exp}$, $\tau_{xz,exp}$, $\tau_{yz,exp}$). SCF5 is the largest root of the polynomial of Eq. (1). The three stress invariants I_e (Eq. [2]), II_e (Eq. [3]), and III_e (Eq. [4]) are determined from the extrapolated stress σ in accordance with Sorensen et al.[5]

$$f(\sigma) = \sigma^3 - I_e\sigma^2 + II_e\sigma - III_e \quad (1)$$

$$I_e = \sigma_{x,exp} + \sigma_{y,exp} + \sigma_{z,exp} \quad (2)$$

$$II_e = \sigma_{x,exp}\sigma_{y,exp} + \sigma_{y,exp}\sigma_{z,exp} + \sigma_{x,exp}\sigma_{z,exp} - \tau^2_{xy,exp} - \tau^2_{xz,exp} - \tau^2_{yz,exp} \quad (3)$$

$$III_e = \sigma_{x,exp}\sigma_{y,exp}\sigma_{z,exp} - \sigma_{x,exp}\tau^2_{yz,exp} - \sigma_{y,exp}\tau^2_{xz,exp} - \sigma_{z,exp}\tau^2_{xy,exp} + 2\tau_{xy,exp}\tau_{xz,exp}\tau_{yz,exp} \quad (4)$$

where

I_e = stress invariant 1

$\sigma_{x,exp}$ = extrapolated normal stress in x-direction

$\sigma_{y,exp}$ = extrapolated normal stress in y-direction

$\sigma_{z,exp}$ = extrapolated normal stress in z-direction

II_e = stress invariant 2

$\tau_{xy,exp}$ = extrapolated shear stress in xy-plane

$\tau_{xz,exp}$ = extrapolated shear stress in xz-plane

$\tau_{yz,exp}$ = extrapolated shear stress in zy-plane

III_e = stress invariant 3

Experimental study

Evaluation of the connection can be achieved through the fabrication of full-sized double-tee members and application of cyclic wheel loads to those members. While this type of test is possible, it is not practical when many tests are required. Furthermore, this type of evaluation will only allow the assessment of the tested connection, embedded in a specific double-tee flange geometry, at a single connector spacing. This type of system test cannot be readily used to determine the performance of variations on the connection such as weld size or location, or to develop rules for other connection types. To provide a comprehensive assessment of this connection detail, a generic subassembly was developed for this weld condition. The failure mode of concern is fatigue-induced fracture of the fillet weld between the jumper plate and connector faceplate. The jumper plate and anchorage of the connector faceplate are relatively stiff. Consequently, the subassembly consists of the flexible portion of the faceplate and the jumper plate (**Fig. 5**).

The fatigue tests were conducted under force control with load cycles from near zero to a predefined force level that generated the target SCF5 stress range. Load was applied at a frequency between 5 and 10 Hz. The experiments were conducted at five laboratories (Lehigh University [LU], University of Akron [UA], University of Illinois at Urbana-Champaign [UI], University of Houston [UH], and Michigan Technological University [MT]).

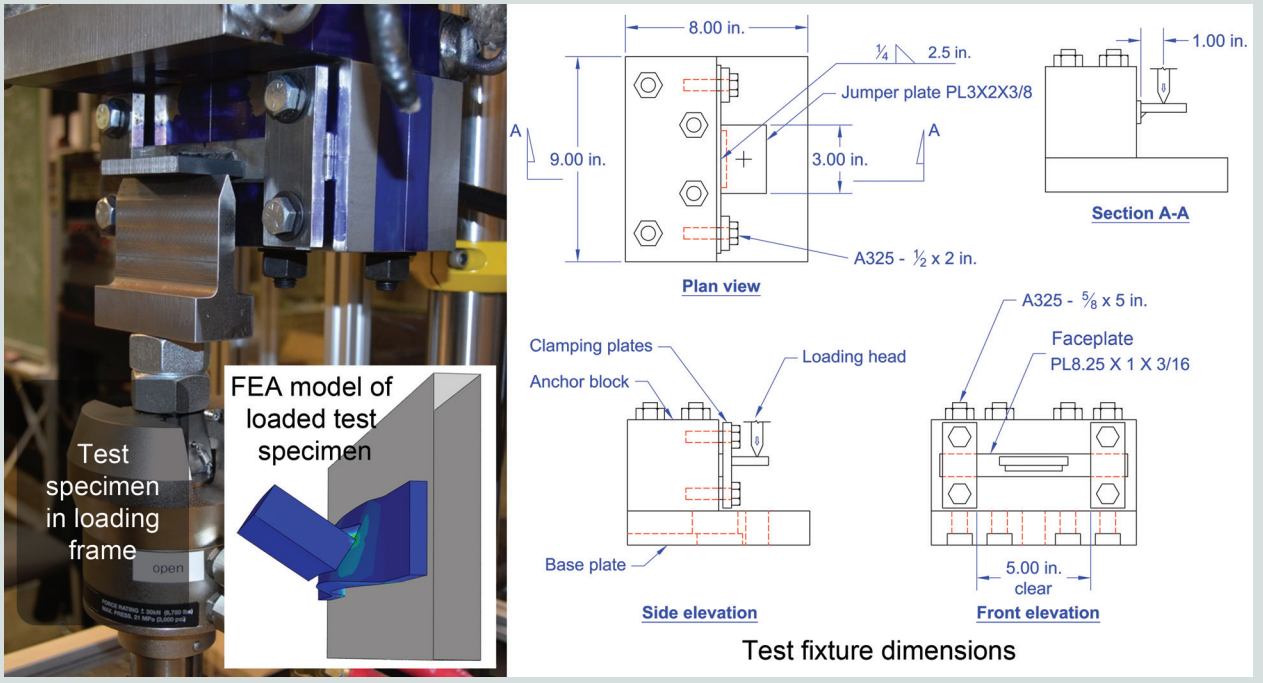

Figure 5. Fatigue loading setup. Note: FEA = finite element analysis. 1 in. = 25.4 mm.

Numerical analysis

Before testing, detailed measurements of the test specimen were taken and each of the 20 test specimens were numerically modeled to determine the required load magnitude to reach a target SCF5 range. The weld throat of the test specimen was measured at 5 to 10 locations along the weld and averaged to determine an average throat size. The weld geometry was idealized as a triangular cross section with a throat dimension equal to the average throat of the specimen. Zero penetration of weld metal into the space between the faceplate and jumper plate was assumed for all cases. The weld length and the size of the plates were determined. The modeling parameters for the SCF5 approach as outlined in Sorensen et al.[5] were followed, except that the element length in the longitudinal direction of the weld was set equal to the weld throat dimension instead of twice the weld throat dimension, to improve accuracy. The SFC5 stress at the root of the weld was calculated at 100 points along the length of the weld in accordance with the procedure previously outlined. **Figure 6** shows a sample plot of the SCF5 results along the length of two specimens. The two specimens were physically similar, but subjected to different loads. The SCF5 stress varies along the length due to the flexibility of the faceplate. Due to the large variation in the magnitude of stress along the length of the weld, the stress was averaged over the entire weld length and the average stress value was used to characterize each test.

Experimental program

The material used for the tests conformed to materials used in fabrication of connectors and field welds. The faceplate material consisted of hot-rolled coil material conforming to HSLA SAE J1392-045XLF.[6] The material had a mill-certified carbon content of 0.060 and a tensile and yield strength of 67.6 and 56.1 ksi (466 and 387 MPa), respectively. The welds were fabricated using the shielded metal arc welding process with AWS E7018 0.125 in. (3.18 mm) electrodes. The jumper plate material was fabricated from ASTM A36 plate.[7] A single pass 0.25 in. (6 mm) fillet weld 2.5 in. (64 mm) long was specified.

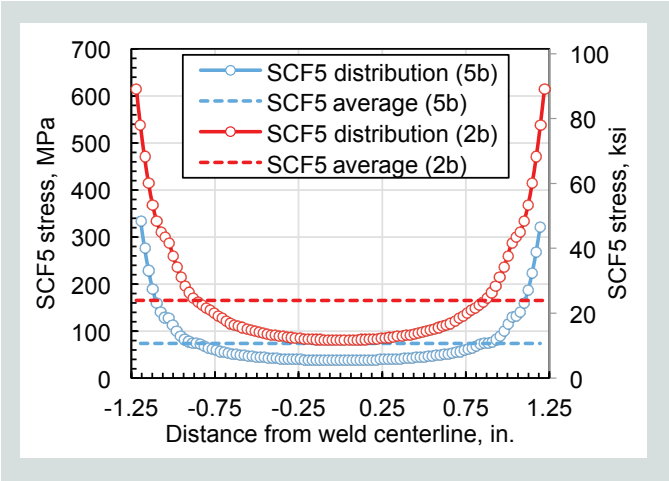

Figure 6. SCF5 stress in welds. Note: SCF5 = stress concentration factor. 1 in. = 25.4 mm.

The actual dimensions of the weld varied considerably and were measured in detail prior to testing, as described previously.

The measured weld details were used with the numerical analysis model to determine the average SCF5 stress range under cyclic loads. Twenty tests were conducted. Five tests were terminated before the onset of fracture. One was stopped before 1 million cycles and four tests were terminated at approximately 20 million cycles. All remaining tests were conducted until failure was observed, defined as fracture of the weld to an extent that further loading was not possible. **Table 1** summarizes the specimen dimensions, applied load, average SCF5 stress, and measured fatigue life, arranged relative to their average SCF5 stress. **Figure 7** shows typical failure surfaces. As indicated by the direction of the ratchet marks shown on the magnified portion of the image and the fatigue striations on the left side of the lower weld, the fatigue failure surfaces started at the ends of the weld and propagated toward the middle. The failure surface was also greater at the ends and smaller at the middle of the weld due to the elevated stress generated from the flexibility of the faceplate (Fig. 6).

The test data were evaluated in accordance with ASTM E739[8] standard practice for statistical analysis of linear stress-life fatigue data. Equation (5) summarizes the resulting data fit for the failure region, along with the test data in **Fig. 8**. An endurance limit of 8.6 ksi (59.3 MPa) was determined by taking an average of the SCF5 values that did not fail by 20 million cycles. The endurance limit represents the average SCF5 value below which fatigue failure is unlikely. Incorporating the endurance limit, the number of cycles to failure was determined in accordance with Eq. (6). The change in the average principal tension stress at the root of the weld is defined as the variable S. Note that in all cases the change in stress is relative to zero stress at the root.

$$\log(N) = 12.698 - 3.323 \log(S) \quad (5)$$

$$N = \begin{cases} 10^{(12.698 - 3.323 \log(S))}, S > 59.3 \text{ MPa} \\ \infty, S \le 59.3 \text{ MPa} \end{cases} \quad (6)$$

where

N = number of cycles

Case study of parking structure

The S-N curve can be used to determine the fatigue life for flange-to-flange connections. Simulated case studies were conducted to illustrate the methodology and to demonstrate the likely fatigue life of a flange-to-flange connection. Two prototype parking decks were examined (**Fig. 9**). Both consisted of 12DT30 double tees with a 1 in. (25.4 mm) gap between tees. The drive aisle was 24 ft (7.3 m) wide and carried vehicles in both directions. The first deck configuration is referred to as the center-heavy connection spacing layout. For this system, a span length of 59 ft 8¼ in. (18.2 m) was used, and connections vary along the length of the joint with three connections centered at the midspan with 3 ft (1 m) spacing. The second deck

Table 1. Weld detail and predicted fatigue life

Test number (laboratory)	Test load, lb	Average throat, in.	Weld length, in.	Average SCF5, ksi	Measured life, *N*
10 (UH)	1003	0.215	2.542	36.06	22,472
2 (LU)	468	0.138	2.480	31.21	81,500
9 (UH)	980	0.229	2.553	31.20	26,810
4 (LU)	402	0.142	2.340	27.51	329,400
3 (LU)	446	0.150	2.430	27.11	254,400
2b (UI)	555	0.189	2.441	23.93	119,329
11 (UA)	502	0.173	2.634	23.25	298,506
6a (MT)	397	0.173	2.524	18.48	1,496,200
7a (UI)	362	0.181	2.609	15.24	568,566
5a (MT)	214	0.130	2.726	14.46	4,676,600
4b (MT)	289	0.170	2.510	14.33	2,121,100
1 (LU)	193	0.150	2.490	11.44	>1,000,000
5b (MT)	220	0.172	2.390	10.69	6,700,000
6b (UI)	289	0.205	2.509	10.65	2,244,684
4a (MT)	216	0.162	2.579	10.53	>20,650,700
3a (UH)	267	0.208	2.566	9.21	2,338,392
3b (UH)	281	0.215	2.557	9.11	1,577,595
2a (UI)	185	0.181	2.415	8.34	>20,000,000
1a (UA)	188	0.197	2.202	8.19	>20,000,000
12 (UA)	195	0.190	2.673	7.35	>20,000,000

Note: LU = Lehigh University; MT = Michigan Technological University; *N* = number of cycles; SCF5 = stress concentration factor; UA = University of Akron; UI = University of Illinois at Urbana-Champaign; UH = University of Houston. 1 in. = 25.4 mm; 1 lb = 4.448 N; 1 ksi = 6.895 MPa.

consisted of a uniform 5 ft (1.5 m) spacing of connections along the double-tee joint and a 60 ft (18 m) span. This configuration is referred to as the uniform connection spacing layout. Two connector types were examined, both completed using a 1.0 in. wide, 0.375 in. (9.53 mm) thick jumper plate, with a 0.25 in. (6 mm) fillet weld. Based on input from the connector manufacturers, a likely placement and size were used. The tops of both connectors were located 0.75 in. (19 mm) from the top of the double-tee flange surface. The top of the jumper plate was located 0.5 and 0.375 in. (13 and 9.53 mm) from the top of the connector faceplate for connectors 1 and 2, respectively. A 3 in. (75 mm) long jumper plate was used for connector 1 and a 4 in. (100 mm) long plate was used for connector 2, consistent with the corresponding manufacturer's recommendations. Both faceplates had a thickness of 0.1875 in. (4.763 mm). Details on connector 1 and connector 2 can be found in the first part of this study.[2]

A range of vehicle sizes were used to examine the fatigue life of the connections in the parking deck. The vehicle

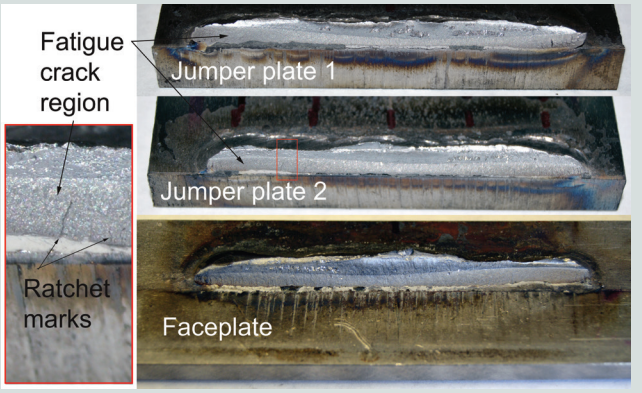

Figure 7. Typical fracture surface of welds.

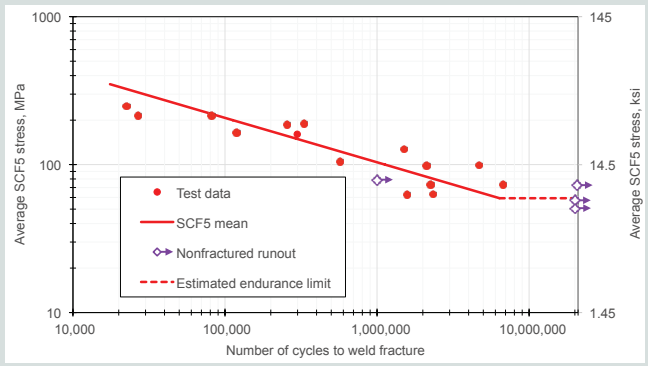

Figure 8. Fillet weld S-N curve. Note: SCF5 = stress concentration factor.

weight distribution was based on a 2001 study of nine parking structures located in Massachusetts and Illinois.[9] Vehicles weights ranged from 1693 to 8600 lb (769 to 3900 kg), with an average weight of 3411 lb (1549 kg). **Figure 10** shows the vehicle distribution size, along with the lognormal distribution recommended by Wen and Yeo.[9] The lognormal distribution had a mean of 8.089 and a standard deviation of 0.304, and was truncated to the interval from 1000 to 8750 lb (450 to 3970 kg). Data on average vehicle weight by vehicle model year have been collated by the Environmental Protection Agency (EPA).[10] The EPA study indicates that the average personal car and truck curb weights increased only 4% since Wen and Yeo conducted their study (from 2001 to 2015, average car weight increased from 3411 to 3617 lb [1549 to 1642 kg] and average truck weight increased from 4543 to 4680 lb [2063 to 2120 kg]). Consequently, the distributions and averages developed for parking structures in 2001 were still applicable at the time of this writing. For simplicity, a standard vehicle footprint was used in our analytical studies. The standard-size vehicle consisted of a track width of 66 in. (1700 mm) and a wheelbase of 105 in. (2670 mm) (Fig. 9). For simplicity, the weight distribution was assumed to be equal to all tire locations. All vehicle loads were applied statically, with no attempt to include dynamic force effects.

Each passage of a vehicle results in two load cycles on the connections at the joint (Fig. 9). The first load cycle occurs when the front axle moves from the near to far side of the joint. The second cycle occurs when the rear axle moves from the near to far side of the joint. The same two-cycle event occurs, albeit in the opposite direction, when the vehicle exits the parking structure. To complicate the analysis, vehicles can drive at any location transverse to the parking structure's deck span. During congested times, when parked cars are present and vehicles are entering and exiting the structure, the moving vehicle will likely be toward the right side of the drive aisle. When the structure is empty and no parking spaces are occupied, the moving vehicle can drive anywhere on the deck,

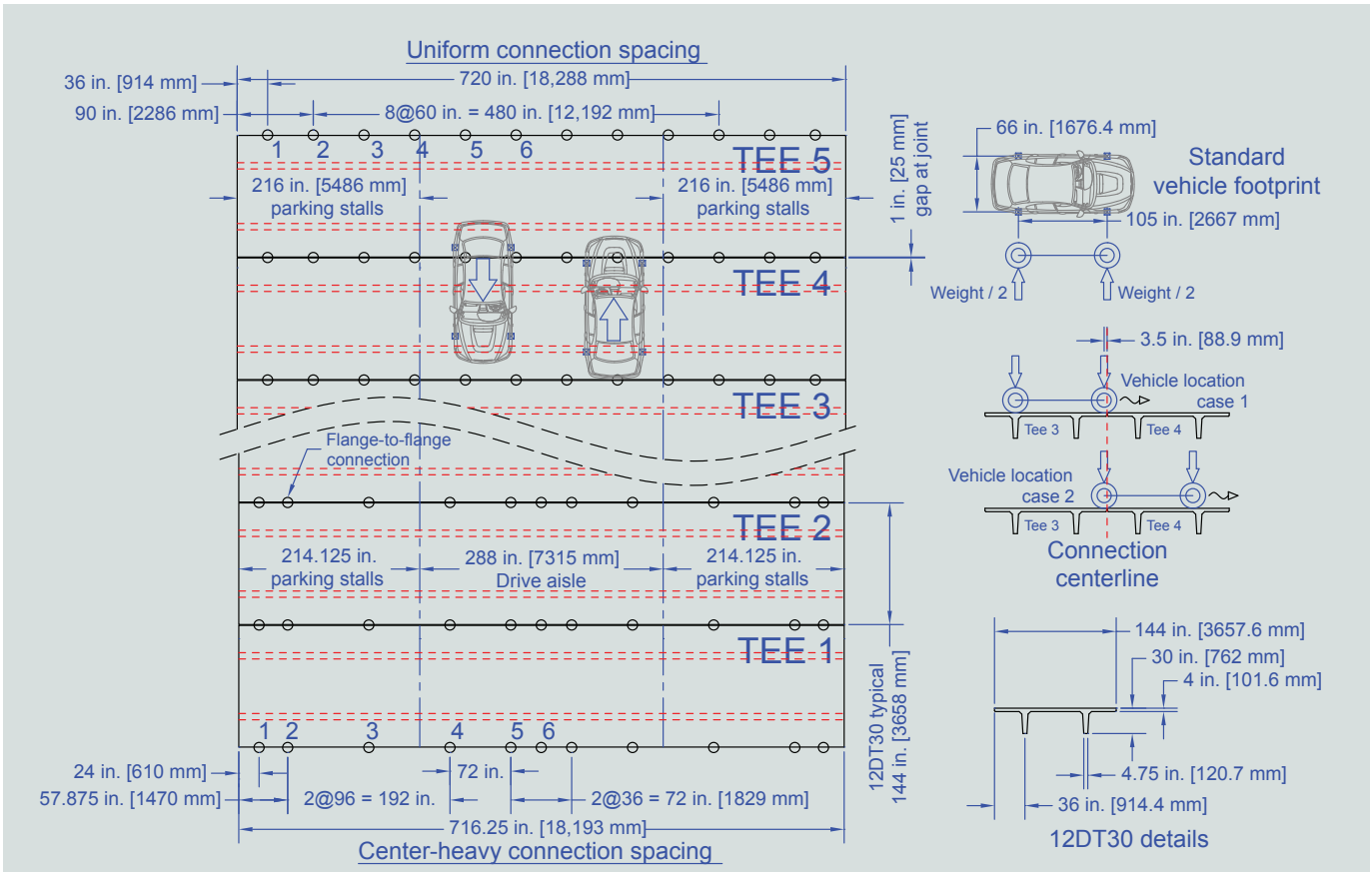

Figure 9. Simulated case study parking structure deck.

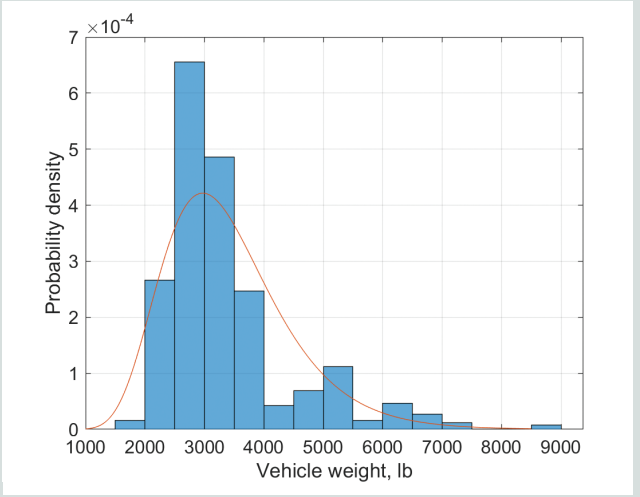

Figure 10. Vehicle weight distribution. Note: 1 lb = 0.454 kg.

including the area reserved for parking stalls. Lastly, when the spaces are occupied and no oncoming cars are present, a driver may likely pass down the center of the drive aisle to maximize the distance from parked cars. The study was conducted with two cases to bound the likely location of vehicle passage within the drive aisle. To represent the most common scenario, a normal distribution was used with a mean occurrence at the center of the drive aisle and a standard deviation of 86 in. (2200 mm). The distribution was truncated to range over the double-tee span (minus half the vehicle track width from each end of the tee) and resulted in approximately 90% of vehicles present in the drive aisle. A secondary scenario was examined where the center of the vehicles can be present anywhere in the 24 ft (7.3 m) drive aisle. For this case, a random distribution was used. **Figure 11** illustrates the two scenarios.

As outlined in Hendricks et al.,[2] two numerical models were developed (**Fig. 12**). The first model consists of a three-dimensional (3-D) finite element model of the connection and the adjacent concrete embedment. The second model consists of a shell model of the parking deck of interest. The 3-D model had to be developed for each connection type of interest and validated with test data. The case study examined two common carbon steel connections that were validated in Hendricks et al. Figure 12 presents the 3-D finite element models of the two connectors. Connector 1 modeled manufacturer 1 and connector 2 modeled manufacturer 2; these are presented in detail in the companion paper.[2]

The 3-D finite element connection model (Fig. 12, left) was used to determine the stiffness of the connection relative to shear, axial, and rotation deformations of the connection. The 3D FEA model of the connection and embedment was developed using commercial software. The concrete embedment and contact were modeled. The 3-D connector mesh was embedded in a 3-D concrete mesh (Fig. 12). Connectivity between the concrete and steel elements was accomplished through nodal ties up to the point where the connector legs return to the face of the concrete. The contact interactions between the jumper plate and connector and between the connector faceplate and concrete were modeled using frictionless "hard" contact. All models were meshed with quadratic brick elements (C3D20) for the connector and jumper plate geometry and with quadratic tetrahedral elements (C3D10) for the concrete. All material properties used in the model were linear elastic. All steel components were modeled with a modulus of elasticity of 29,000 ksi (200,000 MPa) and a Poisson's ratio of 0.3. The concrete was modeled using an elastic modulus of 4700 ksi (32,000 MPa) and a Poisson's ratio of 0.15. **Figure 13** shows the stiffness of the two connections.

The shell model (Fig. 12, right) was used to determine deformation influence lines for vehicle positions along the span. The model uses linear springs developed previously

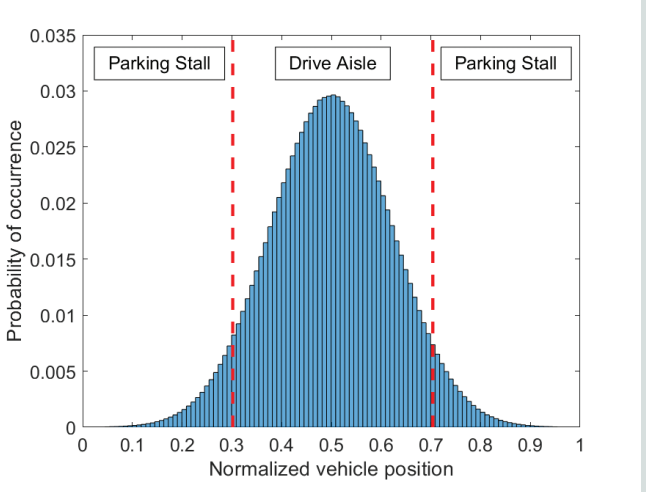

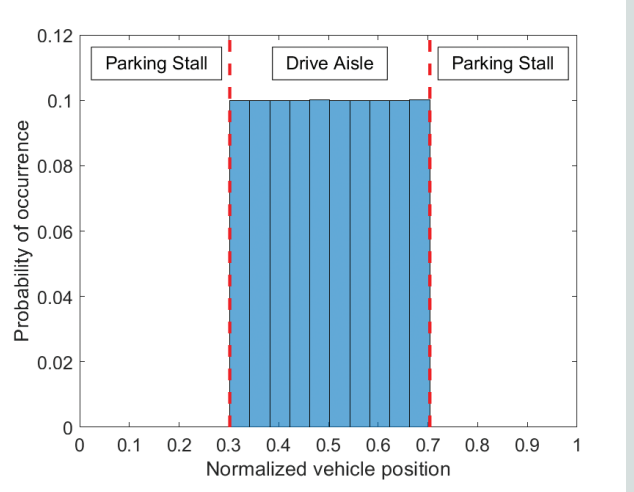

Figure 11. Normal and random vehicle position distribution cases.

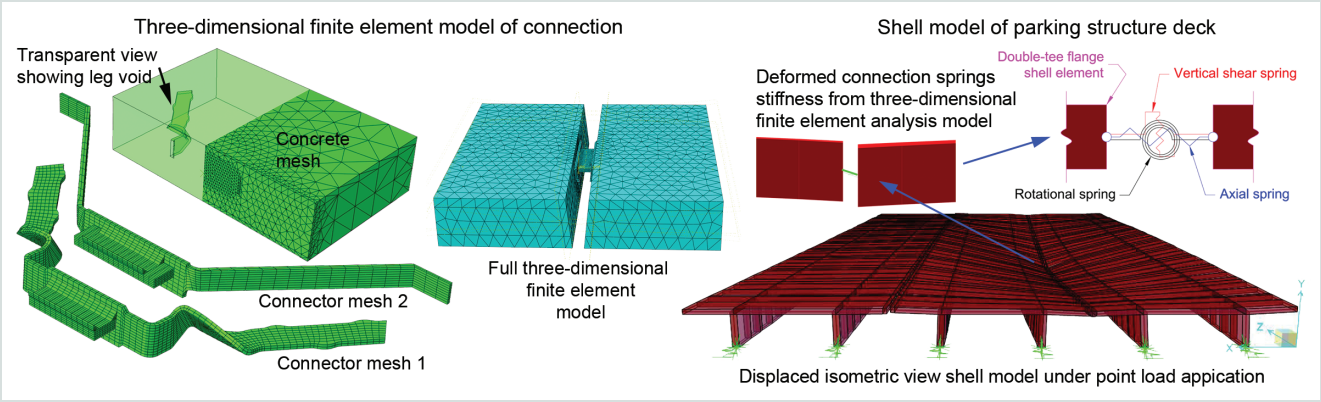

Figure 12. Connection and deck models.

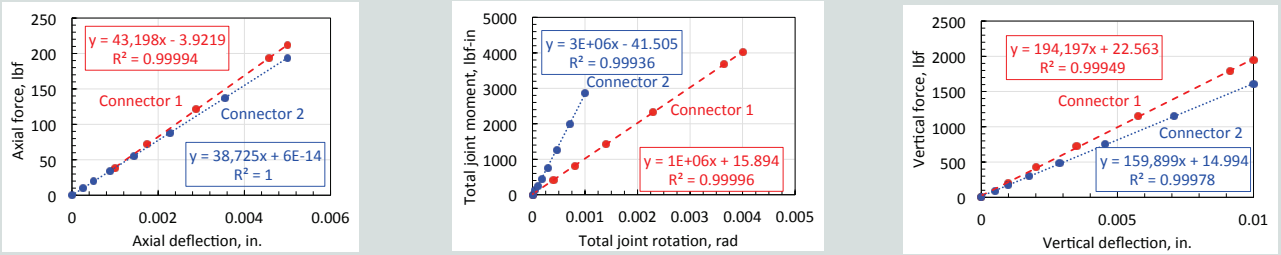

Figure 13. Connection stiffness based on three-dimensional finite element analysis. Note: R^2 = a statistical measure of how close data are to a fitted regression line. 1 in. = 25.4 mm; 1 lbf = 4.448 N.

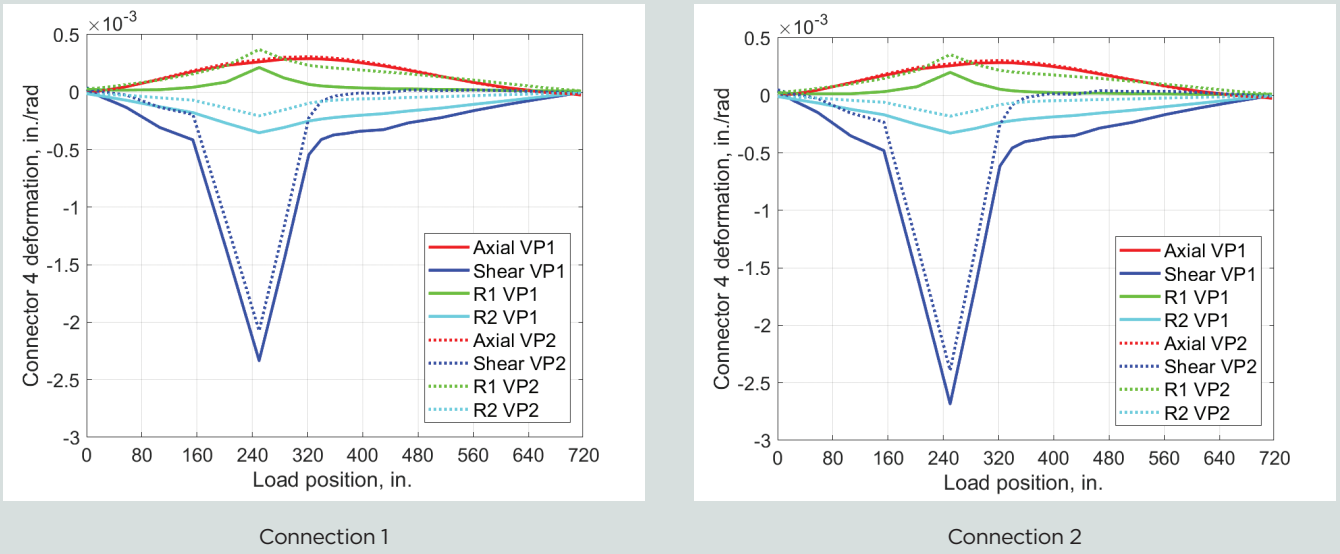

Figure 14. Connection 4 influence lines center-heavy configuration. Note: VP1 = vehicle position case 1; VP2 = vehicle position case 2. 1 in. = 25.4 mm.

in the 3-D model (Fig. 13) for the flange-to-flange connections. The wheel loads can then be applied to the shell model to determine the deformations at any connection along the joint. The influence lines for the four deformations for the vehicle position case 1 (VP1) and vehicle position case 2 (VP2) (Fig. 9) were determined using the shell models. The critical connection for the center-heavy connection arrangement was the connection located 108 in. (2740 mm) from the centerline of the span (connection 4). The offset connection 4 was critical because the close spacing of the three connections at midspan significantly reduced the wheel load demands on the midspan connections. **Figure 14** shows the influence lines for the critical connection in the center-heavy connection configuration. For the uniform connection layout, the midspan connection was the most sensitive to the loading cases. **Figure 15** shows the influence lines for

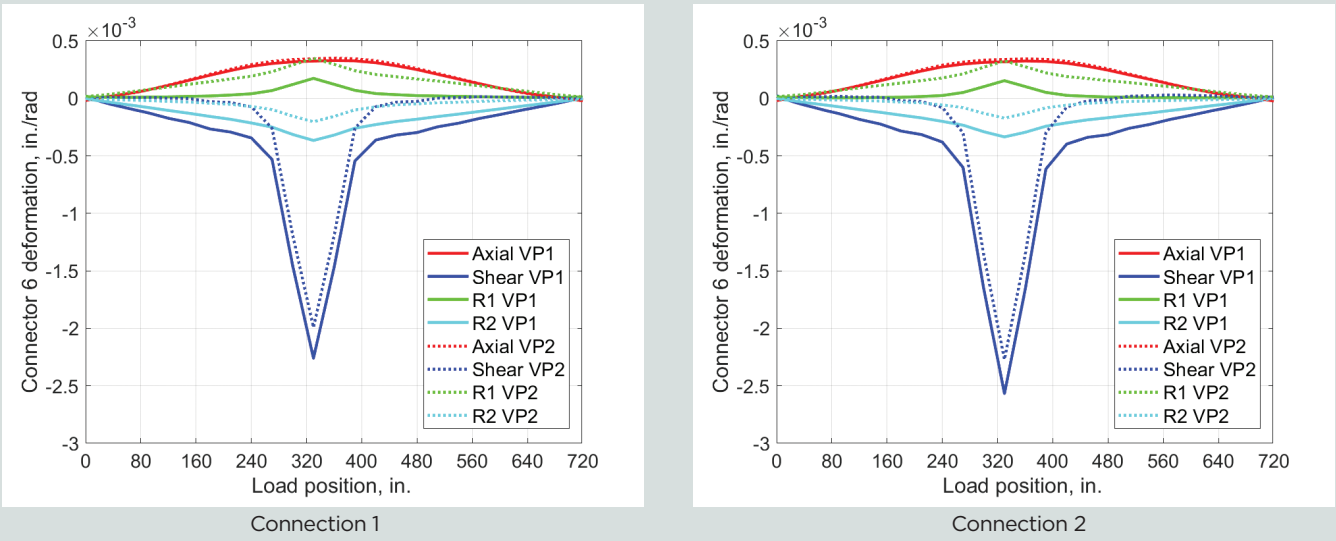

Figure 15. Connection 6 influence lines uniform spacing configuration. Note: 1 in. = 25.4 mm.

the midspan connection in the uniform connector spacing configuration. These influence lines are for a unit load two-wheel vehicle track (that is, one half of the vehicle).

With the response of connection developed and the influence of the connection on the diaphragm performance understood, the average SCF5 root stress can be determined for any vehicle size and location on the floor. Conducting a random sample of vehicle weight and location, the fatigue life of the connection can be determined. **Figure 16** outlines the fatigue analysis procedure.

To facilitate fatigue analysis, superposition of the displacements was used to determine the net root stress for a given load case. The 3-D finite element model was used to examine the correlation between independently applied deformations and combined deformations on the SCF5 stress. The normal distribution of vehicles was placed along the span for vehicle positions 1 and 2. For each case, the corresponding deformations (shear, axial, rotation 1 [flange 1 rotation], and rotation 2 [flange 2 rotation]) at the critical connection were determined. **Figure 17** plots the number of occurrence for each displacement. The deformation corresponding to the most likely occurrence, peak, the maximum deformation observed, max, and two additional levels of likelihood corresponding to midway between the peak and max, mid, and three-quarters of the way from peak to max, mid-max, were determined. Figure 17 shows an example of these points, noted on rotation 1. Each combination of deformations was applied to the 3-D finite element connection model and the SCF5 stress was determined for each case. The deformation values for position 1 and 2, along with their SCF5 values, are summarized for connection 1 (**Tables 2** and **3**) and for connection 2 (**Tables 4** and **5**). A least squares fit was used to determine the relationship between measured deformations at the connection and SCF5 for connection 1 (Eq. [7]) and 2 (Eq. [8]). The resulting SCF5 is in megapascals.

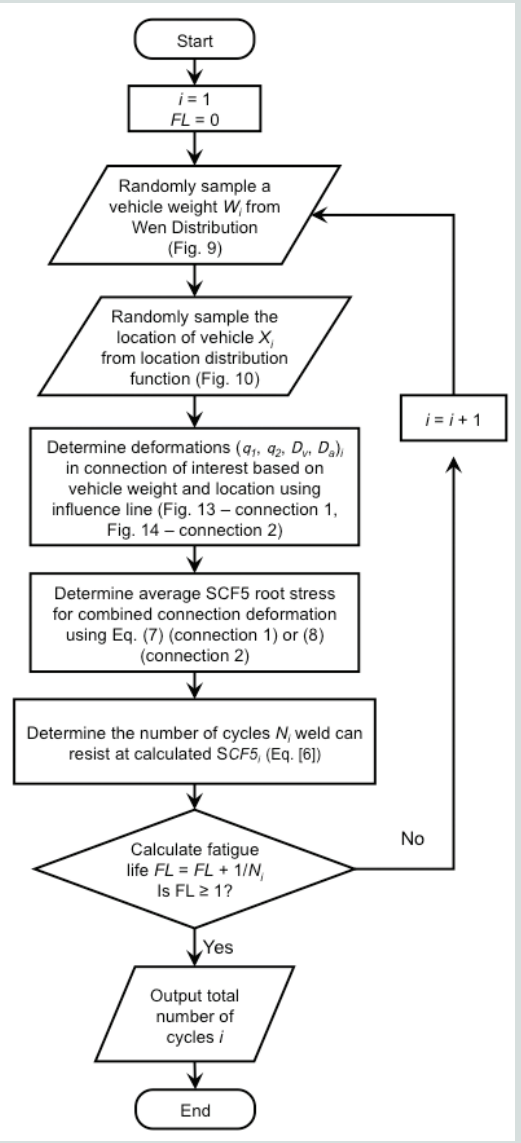

Figure 16. Fatigue evaluation methodology.

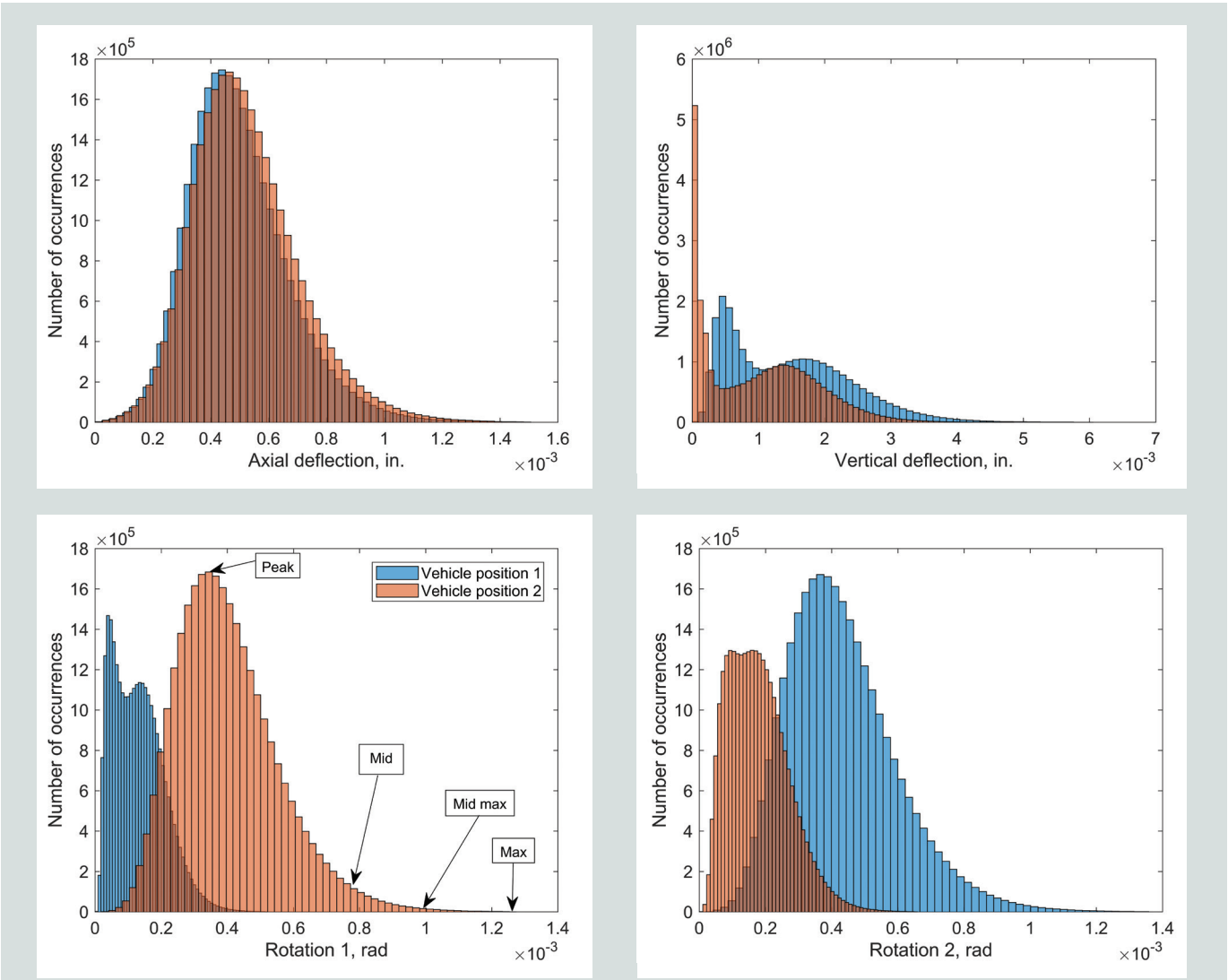

Figure 17. Deformation occurrence at connection 6 for normal distribution of vehicles. Note: SCF5 = stress concentration factor; 1 in. = 25.4 mm.

$$SCF5_1 = -13{,}321\Delta_{axial} + 9384\Delta_{shear} + 48{,}586\theta_1 + 38{,}024\theta_2 \quad (7)$$

$R^2 = 0.994$

$$SCF5_2 = -10{,}825\Delta_{axial} + 11{,}977\Delta_{shear} + 35{,}231\theta_1 + 19{,}494\theta_2 \quad (8)$$

$R^2 = 1.000$

where

Δ_{axial} = axial deflection, in.

Δ_{shear} = vertical deflection, in.

θ_1 = flange 1 rotation, radians

θ_2 = flange 2 rotation, radians

R^2 = a statistical measure of how close data are to a fitted regression line

Case study results

The case studies examined the fatigue life for two vehicle distribution cases, two deck configurations, and two connector types. The analysis was conducted in accordance with the procedure outlined in Fig. 16. The fatigue resistance was calculated relative to a vehicle crossing. A vehicle crossing consists of one pass of the entire vehicle over the joint. This includes the critical loading scenarios of vehicle position case 1 and case 2 (Fig. 9). Using the vehicle weight and position distributions previously discussed, the number of vehicle crossings that can be supported before fatigue-induced fracture of a single connection is expected was determined (**Table 6**).

Due to the close spacing of the connections at midspan in the center-heavy configuration, the connection receiving the greatest demand was connection 4 (Fig. 9). This connection has the highest demand and reaches its fatigue life first for both the normal and random vehicle distribution cases. Because the normal distribution assumes that the mean occurs

Table 2. Uniform 5 ft configuration of connection 1, connector 6 deformations, and corresponding SCF5

Displacement combination	Δ_{axial}, in.	Δ_{shear}, in.	θ_1, rad	θ_2, rad	SCF5, ksi
Vehicle location 1 peak	0.000471	0.000535	0.000151	0.000425	3.255
Vehicle location 1 max	0.001488	0.006420	0.000548	0.001448	18.029
Vehicle location 1 mid	0.000980	0.003478	0.000349	0.000936	9.736
Vehicle location 1 mid-max	0.001234	0.004949	0.000449	0.001192	13.88
Vehicle location 2 peak	0.000500	0.000170	0.000374	0.000156	13.160
Vehicle location 2 max	0.001578	0.005100	0.001346	0.000692	17.518
Vehicle location 2 mid	0.001039	0.002635	0.000860	0.000424	9.350
Vehicle location 2 mid-max	0.001308	0.003868	0.001103	0.000558	13.43

Note: SCF5 = stress concentration factor; Δ_{axial} = axial deflection; Δ_{shear} = vertical deflection; θ_1 = flange 1 rotation; θ_2 = flange 2 rotation. 1 in. = 25.4 mm; 1 ft = 0.305 m; 1 ksi = 6.895 MPa.

Table 3. Center-heavy configuration of connection 1, connector 4 deformations, and corresponding SCF5

Displacement combination	Δ_{axial}, in.	Δ_{shear}, in.	θ_1, rad	θ_2, rad	SCF5, ksi
Vehicle location 1 peak	0.000374	0.000488	0.000064	0.000336	2.947
Vehicle location 1 max	0.001248	0.007320	0.000636	0.001344	19.949
Vehicle location 1 mid	0.000811	0.003904	0.000350	0.000840	10.35
Vehicle location 1 mid-max	0.001030	0.005612	0.000493	0.001092	15.144
Vehicle location 2 peak	0.000374	0.000208	0.000314	0.000087	2.992
Vehicle location 2 max	0.001248	0.006240	0.001344	0.000696	19.711
Vehicle location 2 mid	0.000811	0.003224	0.000829	0.000392	10.28
Vehicle location 2 mid-max	0.001030	0.004732	0.001086	0.000544	14.991

Note: SCF5 = stress concentration factor; Δ_{axial} = axial deflection; Δ_{shear} = vertical deflection; θ_1 = flange 1 rotation; θ_2 = flange 2 rotation. 1 in. = 25.4 mm; 1 ksi = 6.895 MPa.

Table 4. Uniform 5 ft configuration of connection 2, connector 6 deformations, and corresponding SCF5

Displacement combination	Δ_{axial}, in.	Δ_{shear}, in.	θ_1, rad	θ_2, rad	SCF5, ksi
Vehicle location 1 peak	0.00047	0.00196	0.00012	0.00036	4.08
Vehicle location 1 max	0.00140	0.00690	0.00044	0.00124	15.626
Vehicle location 1 mid	0.00093	0.00443	0.00028	0.00080	9.975
Vehicle location 1 mid-max	0.00117	0.00566	0.00036	0.00102	12.78
Vehicle location 2 peak	0.00044	0.00166	0.00032	0.00015	4.035
Vehicle location 2 max	0.00148	0.00552	0.00119	0.00055	14.956
Vehicle location 2 mid	0.00096	0.00359	0.00075	0.00035	9.571
Vehicle location 2 mid-max	0.00122	0.00455	0.00097	0.00045	12.26

Note: SCF5 = stress concentration factor; Δ_{axial} = axial deflection; Δ_{shear} = vertical deflection; θ_1 = flange 1 rotation; θ_2 = flange 2 rotation. 1 in. = 25.4 mm; 1 ft = 0.305 m; 1 ksi = 6.895 MPa.

Table 5. Center-heavy configuration of connection 2, connector 4 deformations, and corresponding SCF5

Displacement combination	Δ_{axial}, in.	Δ_{shear}, in.	θ_1, rad	θ_2, rad	SCF5, ksi
Vehicle location 1 peak	0.00036	0.00056	0.00003	0.00031	1.32
Vehicle location 1 max	0.00120	0.00840	0.00057	0.00126	19.044
Vehicle location 1 mid	0.00078	0.00448	0.00030	0.00078	10.36
Vehicle location 1 mid-max	0.00071	0.00315	0.00020	0.00068	7.328
Vehicle location 2 peak	0.00037	0.00024	0.00027	0.00007	1.30
Vehicle location 2 max	0.00127	0.00720	0.00125	0.00061	18.619
Vehicle location 2 mid	0.00082	0.00447	0.00076	0.00034	11.32
Vehicle location 2 mid-max	0.00105	0.00584	0.00101	0.00048	15.014

Note: SCF5 = stress concentration factor; Δ_{axial} = axial deflection; Δ_{shear} = vertical deflection; θ_1 = flange 1 rotation; θ_2 = flange 2 rotation. 1 in. = 25.4 mm; 1 ksi = 6.895 MPa.

Table 6. Fatigue life of case studies

Deck configuration	Vehicle distribution	Connector type	Number of vehicle crossings
Center-heavy	Normal	1	26,000,000
Center-heavy	Random	1	18,800,000
Uniform	Normal	1	28,700,000
Uniform	Random	1	34,000,000
Center-heavy	Normal	2	32,400,000
Center-heavy	Random	2	22,600,000
Uniform	Normal	2	51,000,000
Uniform	Random	2	60,700,000

at midspan and not at connection 4, the random distribution results in a lower fatigue life for the center-heavy configuration. For the uniform connector spacing this effect reverses. Specifically, for the uniform connection spacing, the midspan connection is the controlling connector. This connection corresponds to the peak location of the normal distribution and thus controls over that of the random case.

Using this fatigue life estimate, the life of connections in the case study parking decks can be determined relative to number of vehicle crossings. **Figure 18** shows the resulting fatigue resistance for both connection arrangements. For the center-heavy connection configuration, the predicted fatigue life for a connection in a heavily used parking structure (500 vehicles in each direction each day, or 1000 vehicle crossings) would be 52 years for connector 1 and 62 years for connector 2. For the uniform connection configuration, the fatigue life for a connection in a heavily used parking structure (500 vehicles in each direction each day, or 1000 vehicle crossings) would be approximately 79 years for connector 1 and 140 years for connector 2. For the cases examined, a fatigue-induced fracture would not be expected for a parking structure with a 50-year design life.

Conclusion

A numerical and experimental study was conducted to examine the fatigue resistance of conventional flange-to-flange double-tee connections subjected to vehicle loading. This paper is the second of a two-part series; part 1 was published in 2018.[2] Based on the study reported here, the following conclusions can be made:

- The fatigue resistance of fillet welds used in flange-to-flange double-tee connections can be assessed through the experimental evaluation of the jumper plate and faceplate of the connection embedded in the double-tee flange.
- The fatigue resistance can be determined from the average principal stress at the root of the weld, SCF5, calculated using a linear extrapolation of the state of stress within the throat of the weld.

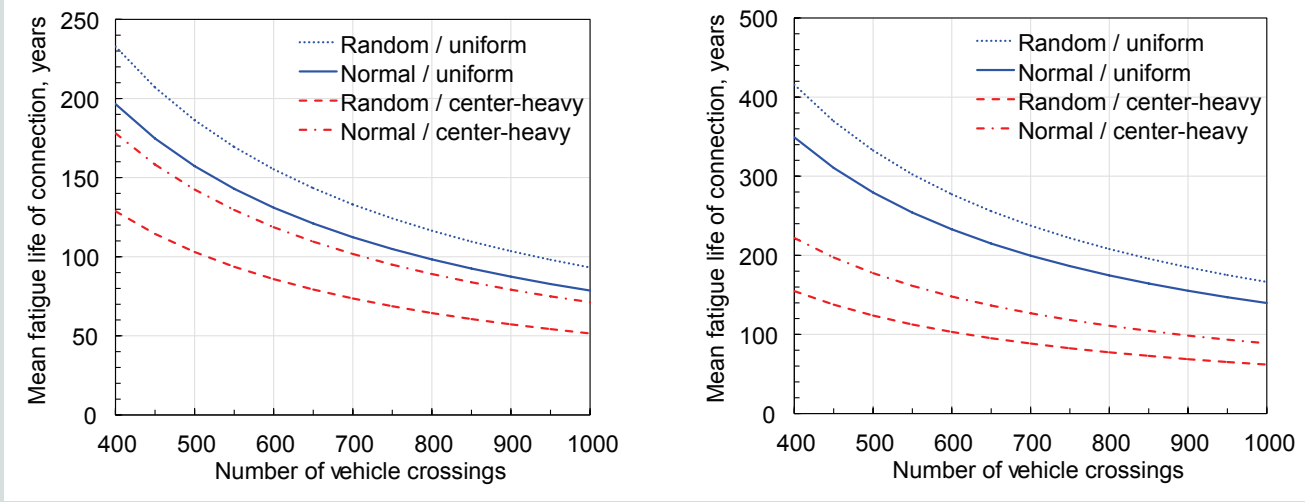

Figure 18. Expected fatigue life of the critical joint connection for case study based on usage.

- The average SCF5 principal stress at the root of the weld is a function of the vertical, axial, and rotational deformations that occur at the connection. The magnitude of deformation at the connection are a function of the vehicle weight, geometry, and location; the connection spacing and stiffness; and the torsional, flexural, and local stiffness of the double-tee flange.

- An S-N curve was developed for the connection. The detail was estimated to have an average SCF5 endurance limit of 8.6 ksi (59.3 MPa).

- Using the S-N curve developed from the experimental testing, simulated case studies were conducted on a 12DT30 diaphragm, with two different connection spacing configurations and two different connector types, with a ⅜ in. (9.5 mm) jumper plate and a ¼ × 3.0 in. (6 × 76 mm) fillet weld with zero penetration. The results show that a heavily used parking structure, supporting 500 vehicles entering and leaving per day for 365 days a year, would theoretically reach 52 to 62 years before a fatigue-induced fracture would be expected to occur. That failure would most likely occur in the drive aisle near the entrance to the parking structure because that is the location most frequently loaded by vehicles.

- Based on the limited study presented, fatigue-induced fracture is sensitive to the connection type and the connection spacing used along the joint. The use of a 6 ft (1.8 m) spacing over a 5 ft (1.5 m) spacing within the drive aisle decreased the fatigue life from 79 to 52 years for connector 1 and from 140 to 62 years for connector 2. Maintaining a closer spacing at joint locations within the drive aisle will improve the fatigue life.

The approach developed in this paper can be extended to other connection details through finite element modeling of the various connection geometries. It can also be extended to other diaphragm configurations through modeling of variations of connection spacing, stiffness, and double-tee geometry. Some conservative simplifications were made in the analysis that can be refined if additional accuracy is needed. For example, all vehicles were assumed to have the same track and axle widths. This is not actually the case, as a lighter-weight vehicle would likely have a smaller wheelbase while a larger vehicle would have a larger wheelbase. The impact of these variations on the fatigue life is unclear.

The scope of the study was limited to the two connection configurations detailed in this paper. No lower-bound fatigue performance was provided due to the limited tests conducted. Although the results presented are representative of a large proportion of connections in use, variations in the parameters studied would alter the performance. The results are sensitive to changes in the connector geometry, connector materials, weld materials, weld size, jumper plate geometry, double-tee size, and connection spacing used. Additional research is recommended to examine the impact of weld size, weld location, construction tolerances, connection spacing, double-tee size, and weld penetration on the fatigue life. Further work is also recommended to examine corrosion fatigue and the impact of thermal effects on the fatigue life. Thermal effects could include the potential for embrittlement of the connection at low temperatures and nonzero mean stress in the weld due to axial forces due to thermal variation in the floor.

Acknowledgments

The authors would like to recognize that the experimental studies conducted as part of this research effort were funded by PCI. The experimental tests conducted in this study were executed by researchers at Lehigh University in Bethlehem, Pa.; University of Akron in Ohio; University of Illinois at Urbana-Champaign; University of Houston in Texas; and Michigan Technological University in Houghton. Connector hardware material was donated by several manufacturers. Many individuals contributed to the research effort, including Roger Becker, Ned Cleland, Larbi Sennour, Harry Gleich, Chuck Wynings, Chuck Magnesio, Eisa Rahmani, Steven Altstadt, and Don Meinheit.

References

1. Ghosh, S. K., N. M. Cleland, and C. J. Naito. 2018. *Seismic Design of Precast Concrete Diaphragms: A Guide for Practicing Engineers*. NEHRP Seismic Design Technical Brief No. 13, NIST GCR 17-917-47. Gaithersburg, MD: National Institute of Standards and Technology. https://doi.org/10.6028/NIST.GCR.17-917-47.

2. Hendricks, R., C. Naito, and A. Osborn. 2018. "Flange-to-Flange Double-Tee Connections Subjected to Vehicular Loading, Part 1: Numerical Assessment Approach." *PCI Journal* 63 (4): 41–53.

3. AISC (American Institute for Steel Construction). 2016. *Specification for Structural Steel Buildings*. ANSI/AISC 360-16. Chicago: IL: AISC.

4. Dimitrakis, S. D. 1999. "Improving the Fatigue Life Weldments with Longitudinal Attachments." PhD diss., University of Illinois at Urbana-Champaign.

5. Sorensen, J. D., J. Tychsen, J. U. Andersen, and R. D. Brandstrup. 2006. "Fatigue Analysis of Load-Carrying Fillet Welds." *Journal of Offshore Mechanics and Arctic Engineering* 128 (1): 65–74. https://doi.org/10.1115/1.2163876.

6. SAE International. 2001. *Steel, High Strength, Hot Rolled Sheet and Strip, Cold Rolled Sheet, and Coated Sheet*. SAE J1392-2001. Warrendale, PA: SAE International.

7. ASTM Subcommittee A01.02. 2014. *Standard Specification for Carbon Structural Steel*. ASTM A36/A36M-14. West Conshohocken, PA: ASTM International. https://doi.org/10.1520/A0036_A0036M-14.

8. ASTM Subcommittee E08.04. 2015. *Standard Practice for Statistical Analysis of Linear or Linearized Stress-Life (S-N) and Strain-Life (ε-N) Fatigue Data*. ASTM E739-10. West Conshohocken, PA: ASTM International. https://doi.org/10.1520/E0739-10R15.

9. Wen, Y. K., and G. L. Yeo. 2001. "Design Live Loads for Passenger Cars Parking Garages." *Journal of Structural Engineering* 127 (3): 280–289.

10. U.S. Environmental Protection Agency (EPA). 2016. *Light-Duty Automotive Technology, Carbon Dioxide Emissions, and Fuel Economy Trends: 1975 Through 2016*. EPA-420-R-16-010. Washington, D.C.: EPA.

Notation

A = quarter point (located closer to the root of the weld) along a line that radiates from the root of the weld to the face of the weld

B = quarter point (located closer to the face of the weld) along a line that radiates from the root of the weld to the face of the weld

I_e = stress invariant 1

II_e = stress invariant 2

III_e = stress invariant 3

N = number of cycles

R^2 = a statistical measure of how close data are to a fitted regression line

S = change in the average principal tension stress at the root of the weld

S_A = average principal tension stress at the root of the weld at point A

S_B = average principal tension stress at the root of the weld at point B

S_{exp} = extrapolated average principal tension stress at the root of the weld

t = thickness of weld throat

Δ_{axial} = axial deflection

Δ_{shear} = vertical deflection

σ = stress

σ_x = normal stress in x-direction

$\sigma_{x,exp}$ = extrapolated normal stress in x-direction

σ_y = normal stress in y-direction

$\sigma_{y,exp}$ = extrapolated normal stress in y-direction

σ_z = normal stress in z-direction

$\sigma_{z,exp}$ = extrapolated normal stress in z-direction

τ_{xy} = shear stress in xy-plane

$\tau_{xy,exp}$ = extrapolated shear stress in xy-plane

τ_{xz} = shear stress in xz-plane

$\tau_{xz,exp}$ = extrapolated shear stress in xz-plane

τ_{zy} = shear stress in zy-plane

$\tau_{yz,exp}$ = extrapolated shear stress in zy-plane

θ_1 = flange 1 rotation

θ_2 = flange 2 rotation